


Cite this: *RSC Adv.*, 2024, 14, 16401

# A novel magnetic FSM-16 supported ionic liquid/Pd complex as a high performance and recyclable catalyst for the synthesis of pyrano[3,2-c]chromenes†

Azar Jahanbakhshi and Mahnaz Farahi \*

In this work,  $\text{Fe}_3\text{O}_4\text{@FSM-16/IL-Pd}$  was successfully designed and synthesized via a new procedure of palladium(II) complex immobilization onto magnetic FSM-16 using an ionic liquid, as a novel heterogeneous nanocatalyst. Multiple techniques were employed to characterize this magnetic nanocatalyst such as Fourier transform infrared spectroscopy (FT-IR), Brunauer–Emmett–Teller (BET), X-ray diffraction (XRD), energy-dispersive X-ray spectroscopy (EDS), Field Emission Scanning Electron Microscopy (FE-SEM), thermogravimetric analysis (TGA), Transmission electron microscopy (TEM), and Vibrating Sample Magnetometry (VSM). After complete characterization of the catalyst, its catalytic activity was used for the synthesis of pyrano[3,2-c]chromene-3-carbonitriles via the reaction of 4-hydroxycoumarin, aldehyde, and malononitrile under solvent-free conditions. Also, it can be recovered and reused several times without a significant decrease in its catalytic activity or palladium leaching.

Received 22nd February 2024  
Accepted 13th May 2024

DOI: 10.1039/d4ra01381f

rsc.li/rsc-advances

## 1. Introduction

Chromene derivatives are oxygen-containing heterocyclic compounds with diverse pharmaceutical and biological properties which are widely distributed in nature.<sup>1–3</sup> Chromenes demonstrate a diverse range of biological activities, such as anti-anaphylactic activity, antimicrobial, anticancer properties, diuretic, and spasmolytic, and are also used to synthesize tacrine analogs and the blood anticoagulant warfarin.<sup>4,5</sup> Chromene derivatives also form components of many natural products such as calanolides, calophyllolide, and calanone.<sup>6</sup> In addition, pyrano[3,2-c]chromenes exhibit a wide range of biological activities, including against Alzheimer's disease, schizophrenia, and AIDS-associated dementia, making them valuable synthons for the synthesis of pharmacological agents.<sup>7</sup> The main method for their preparation is the one-pot three-component reaction of 4-hydroxycoumarin with aldehyde and malononitrile in the presence of a catalyst. Consequently, a wide range of catalysts have been explored for the synthesis of pyrano[3,2-c]coumarins, including  $\text{t-ZrO}_2$  NPs,<sup>8</sup> SB-DABCO@eosin,<sup>9</sup>  $\text{Fe}_3\text{O}_4\text{@GO-NH}_2$ ,<sup>10</sup> chitosan-Zn,<sup>11</sup> L-proline,<sup>12</sup>  $\text{rGO@Fe}_3\text{O}_4\text{@ZrCp}_2\text{Cl}$ ,<sup>13</sup> and many others. However, many existing methods for the synthesis of these compounds exhibit limitations such as low yields of the product, relying on multi-

step conditions, high reaction time, very expensive reagents, poor recovery of the catalyst, the use of toxic organic solvents, and a tedious work-up procedure. Due to these limitations, the development of efficient, simple, and environmentally benign processes for the synthesis of pyran derivatives remains a critical objective aligned with green chemistry principles.<sup>14,15</sup>

The design and development of novel catalysts with excellent activity, selectivity, and resistance to deactivation is one of the primary objectives of research scientists in the long term. Catalysts can typically be classified into two main categories: homogeneous and heterogeneous catalysts.<sup>16,17</sup> The use of homogeneous catalysts is restricted due to various issues, including poisoning, the generation of toxic metal waste, catalyst leakage, high costs, non-recyclability, and time-consuming processes that result in impurities in the final products.<sup>18–20</sup> Therefore, the problems mentioned above can be overcome by using heterogeneous catalysts. Heterogeneous catalysts provide significant advantages such as recoverability, high stability, ease of handling, prevention of metal loss, and reduced environmental impact. However, they also have some disadvantages, such as less contact between the raw material and the catalyst, the separation of active species from the surface of the catalyst, and the problem of transferring energy and heat to perform the reaction.<sup>21,22</sup> The use of solid heterogeneous catalysts in organic reactions is crucial to achieving environmentally sustainable and effective catalytic processes due to their widespread application in environmentally friendly chemical processes. During the past few decades, stabilized metallic nanoparticles have been utilized as heterogeneous catalysts in

Department of Chemistry, Yasouj University, Yasouj, Iran, 75918-74831. E-mail: farahimb@yu.ac.ir; Fax: +98 7412242167e

† Electronic supplementary information (ESI) available. See DOI: <https://doi.org/10.1039/d4ra01381f>



the transformation of organic functional groups and novel organic synthesis.<sup>23</sup> Some of the important works reported on the synthesis of Pd metallic nanoparticles are  $\text{Fe}_3\text{O}_4@\text{DAG}/\text{Pd}$ ,<sup>24</sup>  $\text{Fe}_3\text{O}_4@\text{void}@\text{C-Schiff-base}/\text{Pd}$ ,<sup>25</sup> *hercynite*@L-methionine-Pd MNPs,<sup>26</sup>  $\text{PdNPs}@\text{[KIT-6]-PEG-imid}$ ,<sup>27</sup> and  $\text{HNT}/\text{C}@\text{Pd}$  NPs.<sup>28</sup> Among various metal and metal oxide nanoparticles,  $\text{Fe}_3\text{O}_4$  magnetic oxide nanoparticles (MNPs) owing to their inherent properties including superparamagnetism, a significant surface area, low toxicity, easy separation, recyclability through an external magnetic field, and reuse in chemical processes have garnered significant attention.<sup>29–31</sup> However, the utilization of these nanoparticles is hampered by their instability in acidic and alkaline environments, the tendency to aggregate and deform in some organic solvents, and easy oxidation.<sup>32,33</sup> Therefore,  $\text{Fe}_3\text{O}_4$  magnetic nanoparticles are coated with a range of materials, including mesoporous silica materials,<sup>34–36</sup> polymers,<sup>37</sup> carbon nanotubes,<sup>38</sup> cellulose,<sup>39,40</sup> graphene oxide,<sup>41</sup> biochar,<sup>42</sup> and boehmite nanoparticles,<sup>43</sup> resulting in the formation of core-shell structures. These coatings may enhance the stability, performance, and biocompatibility, making them suitable for various applications in nanocatalysts, biomedicine, and nanotechnology.<sup>44,45</sup> Hence, the utilization of nanoscale mesoporous silica materials with chemical and thermal stability and high surface area to coat  $\text{Fe}_3\text{O}_4$  NPs is particularly attractive. Some of the recently synthesized magnetic mesoporous nanocatalysts are  $\text{Fe}_3\text{O}_4@\text{SiO}_2@\text{PMO}$ ,<sup>46</sup>  $\text{MCM-48-CoFe}_2\text{O}_4-\text{NH}_2$ ,<sup>47</sup>  $\text{Fe}_3\text{O}_4\text{NPs}@\text{ME}$ ,<sup>48</sup> and  $\text{Fe}_3\text{O}_4@\text{SiO}_2@\text{SBA-15}$ .<sup>49</sup>

Among mesoporous silica compounds, FSM-16 (Folded Sheet Mesoporous) has attracted much interest due to its high pore volume, large surface area, surface silanol groups, and uniform pore diameter.<sup>50</sup> FSM-16 structures are prepared by intercalating a quaternary ammonium surfactant template into layered sodium silicate (kanemite). Calcination removes the template, resulting in the formation of a mesoporous channel structure with a hexagonal arrangement. Their pore sizes range from 2 to 50 nanometers. FSM-16 has attracted many applications in the fields of catalytic chemistry, drug delivery, adsorption science, chromatography, and electrodes.<sup>51,52</sup> Some of the most recently studied nanocatalyst for FSM-16 including  $\text{Fe}_3\text{O}_4@\text{FSM-16-SO}_3/\text{IL}$ ,<sup>53</sup>  $\text{FSM-16}@\text{imine-thiophen}/\text{Pd}$ ,<sup>54</sup>  $\text{FSM-16-IL-SO}_3\text{H}$ ,<sup>55</sup>  $\text{FSM-16/CPTMS-Rh-Ni(II)}$ ,<sup>56</sup>  $\text{Fe}_3\text{O}_4@\text{FSM-16-SO}_3\text{H}$ ,<sup>57</sup>  $\text{FSM-16-Met}$ ,<sup>58</sup> and  $\text{FSM-16-SO}_3\text{H}$ .<sup>59</sup>

Ionic liquids have attractive properties such as low vapor pressure, non-flammability, high viscosity, non-volatility, high thermal stability, high catalytic activity, recyclability, and eco-friendliness. However, the liquid state and the high viscosity of ionic liquids limit their ability to be separated and recycled in catalytic reactions.<sup>60,61</sup> An attractive approach for the fabrication of an effective solid catalyst, and recyclable is the covalent stabilization of ionic liquids on a heterogeneous solid surface, such as a suitable magnetic mesoporous. Common types of ionic liquids covalently attached to heterogeneous surfaces include aliphatic quaternary amines, thiazolium, imidazolium, and hexamethyltetraaminium (HMTA).<sup>62–64</sup> These materials are promising candidates for transition metal support, gas separation, water treatment, and catalysis.<sup>65</sup> Many ionic liquids stabilized on magnetic mesoporous materials have been

applied in chemical reactions, such as  $\text{Fe}_3\text{O}_4/\text{Hal-Mel-TEA(IL)-Pd}$ ,<sup>66</sup>  $\text{Mag-IL-Pd}$ ,<sup>67</sup>  $\text{FSS-IL}$ ,<sup>68</sup>  $\text{Zn}_{0.2}\text{Fe}_{2.8}\text{O}_4@\text{SBA-15}_{0.5}@\text{CH}_3\text{COO}$ ,<sup>69</sup>  $\text{POMs-ILs}@\text{MOF}$ ,<sup>70</sup> and  $\text{SiO}_2@\text{Pd(R)}/\text{Fe-MS}$ .<sup>71</sup>

In this research,  $\text{Fe}_3\text{O}_4@\text{FSM-16}/\text{IL-Pd}$  core-shell nanocatalyst was prepared and characterized by various analyses.  $\text{Fe}_3\text{O}_4@\text{FSM-16}/\text{IL-Pd}$  was used as a heterogeneous and efficient catalyst for the preparation of pyrano[3,2-*c*]chromene-3-carbonitrile derivatives.

## 2. Experimental

### 2.1. Materials

All of the reagents, solvents, and chemicals including tetraethyl *ortho* silicate (TEOS), cetyltrimethyl ammonium bromide (CTAB), sodium hydroxide (NaOH),  $\text{FeCl}_3 \cdot 6\text{H}_2\text{O}$ ,  $\text{FeCl}_2 \cdot 4\text{H}_2\text{O}$ , 1,4-diazabicyclo[2.2.2]octane (DABCO), 3-chloropropyltrimethoxysilane (CPTMS),  $\text{PdCl}_2$ , 4-hydroxycoumarin, malononitrile, benzaldehyde, 3-bromobenzaldehyde, 2-chloro-3-fluorobenzaldehyde, 4-cyanobenzaldehyde, 3-ethoxy-4-hydroxyphenylbenzaldehyde, 4-isopropylbenzaldehyde, 1-naphthaldehyde, 4-(benzyloxy)benzaldehyde, cyclohexanecarbaldehyde, ethanol, toluene, DMF, DMSO were purchased from Merck (Germany) and Fluka (Switzerland), and were used without any further purification.

**2.1.1. Synthesis of  $\text{Fe}_3\text{O}_4@\text{FSM-16}$ .** The  $\text{Fe}_3\text{O}_4$  was synthesized according to the literature procedure. A solution of sodium hydroxide (3 g) in deionized water (30 mL) was prepared. Tetraethyl *ortho* silicate (TEOS) (16.6 mL) was slowly added dropwise to the NaOH solution over a 1 h period. The resulting mixture was then stirred for 24 h at 80 °C. After stirring, the mixture was centrifuged to separate the solid material. The solid was then washed with deionized water to remove any impurities. Finally, the washed solid was dried in an oven at 80 °C for 12 h. To complete the synthesis of kanemite ( $\delta\text{-Na}_2\text{Si}_2\text{O}_5$ ), the dried material was calcined at a temperature of 650 °C for 5 h. 5 g of the synthesized kanemite were added to 50 mL of deionized water. The mixture was stirred for 3 h at 30 °C. The suspension was then filtered to obtain the wet kanemite dough. In the following,  $\text{Fe}_3\text{O}_4$  nanoparticles (0.106 g, 0.457 mmol) were first dispersed in 50 mL of deionized water using ultrasonic waves. To improve dispersion, cetyltrimethylammonium bromide (CTAB) was then added by slowly raising the temperature to 70 °C. Then, the kanemite paste was added and then stirred at 70 °C for 3 h. At this stage, the pH value of the suspension was 11.5–12.5. After 3 h, the pH of the medium was adjusted to 8.5 with HCl (2 M), and the mixture was stirred at 70 °C for another 3 h. Once the mixture cooled down, the resulting solid particles were separated using centrifugation, and washed with deionized water. The magnetite mesoporous silicate ( $\text{Fe}_3\text{O}_4@\text{FSM-16}$ ) was isolated as a final product through a two-step process. First, it was dried in an oven at 80 °C for 2 h to remove any remaining water. Subsequently, it underwent calcination at 650 °C for 5 h to burn the surfactant and synthesis of the final magnetite mesoporous silicate,  $\text{Fe}_3\text{O}_4@\text{FSM-16}$ .<sup>53</sup>

**2.1.2. Synthesis of  $\text{IL}_{\text{DABCO}}$  (bis-PrSi/DABCO/Cl).**  $\text{IL}_{\text{DABCO}}$  (bis-PrSi/DABCO/Cl) was prepared according to the method



described by Kiasat *et al.*<sup>72</sup> Firstly, 1,4-diazabicyclo[2.2.2]octane (DABCO) (0.8 mmol) was mixed with 3-chloropropyltrimethoxysilane (CPTMS) (16 mmol) in DMF (30 mL) under N<sub>2</sub> atmosphere for 72 h at 90 °C. The resulting white solid, bis-PrSi/DABCO/Cl, was separated by filtration, washed with MeOH, and dried in an oven at 90 °C for 2 h.

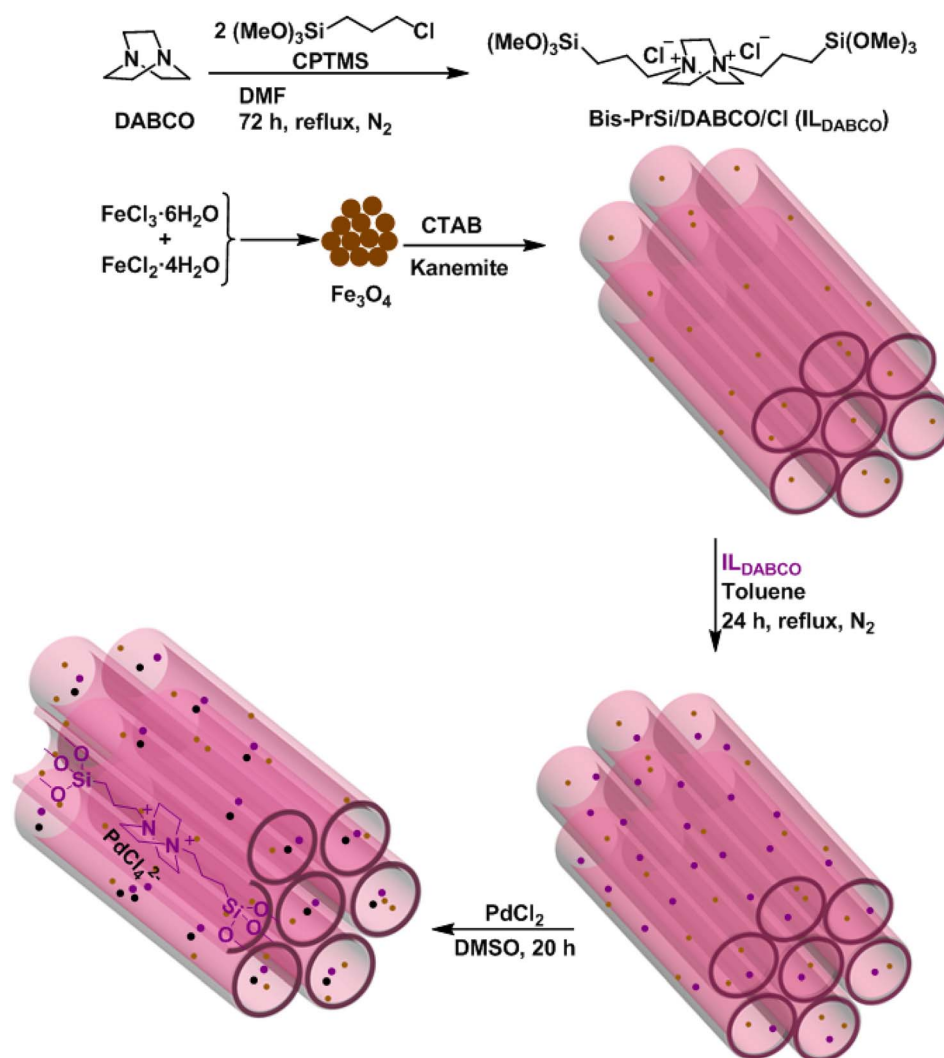
**2.1.3. Synthesis of Fe<sub>3</sub>O<sub>4</sub>@FSM-16/ILDABCO.** Next, to prepare Fe<sub>3</sub>O<sub>4</sub>@FSM-16/IL, magnetic Fe<sub>3</sub>O<sub>4</sub>@FSM-16 nanoparticles (0.25 g) were added to dry toluene (30 mL) and dispersed at room temperature for 30 min. Then, bis-PrSi/DABCO/Cl (0.33 mmol) was added and the resulting mixture was refluxed under an N<sub>2</sub> atmosphere for 24 h. Finally, to obtain Fe<sub>3</sub>O<sub>4</sub>@FSM-16/IL, the brown solid was separated with an external magnet, washed several times with ethanol, and dried in an oven at 80 °C for 2 h.

**2.1.4. Synthesis of Fe<sub>3</sub>O<sub>4</sub>@FSM-16/IL-Pd nanocatalyst (1).** Finally, to immobilize PdCl<sub>2</sub> on Fe<sub>3</sub>O<sub>4</sub>@FSM-16/IL nanoparticles, Fe<sub>3</sub>O<sub>4</sub>@FSM-16/IL (0.5 g) was dispersed in DMSO (30 mL) for 30 min. Then, PdCl<sub>2</sub> (0.2 g) was added to the reaction mixture and stirred for 20 h at room temperature. The resulting

product, designated Fe<sub>3</sub>O<sub>4</sub>@FSM-16/IL-Pd nanocatalyst, was magnetically separated, washed with EtOH, and dried at 70 °C for 3 h.

## 2.2. Instrumental

The Fourier Transform Infrared spectrum was performed in the range 400–4000 cm<sup>−1</sup> using a PerkinElmer Spectrum 2, USA instruments. NMR spectra were recorded on a Bruker 400 MHz Ultrashield spectrometer at 400 MHz (<sup>1</sup>H) and 100 MHz (<sup>13</sup>C) using DMSO-*d*<sub>6</sub> as solvent. The structure of the nanocatalyst was recognized by X-ray diffraction (XRD) measurements (Rigaku Ultima IV, Japan). Field emission-scanning electron microscopy (FE-SEM) images were taken using the FE-SEM TESCAN MIRA3. Transmission electron microscopy (TEM) images were examined using a Philips EM208S apparatus. The energy dispersive X-ray (EDX) spectrum was measured using a TESCAN VEGA model of the instrument. Thermogravimetric analysis (TGA) of the catalyst was performed using a PerkinElmer STA 6000 instrument. The N<sub>2</sub> adsorption–desorption isotherm was performed to determine the specific surface areas by Brunauer–Emmett–Teller (BET)



Scheme 1 Synthesis of Fe<sub>3</sub>O<sub>4</sub>@FSM-16/IL-Pd nanocatalyst 1.

(BELSORP miniII, Japan). Vibration Sample Magnetometry (VSM) was studied by the Kavir Magnet VSM.

## 2.3. Catalytic tests

**2.3.1. General procedure for the synthesis of pyrano[3,2-*c*]chromene-3-carbonitrile derivatives.** A mixture of aldehyde (1 mmol), malononitrile (1 mmol), 4-hydroxycoumarin (1 mmol), and  $\text{Fe}_3\text{O}_4@\text{FSM-16}/\text{IL-Pd}$  (0.006 g) was stirred at 70 °C under solvent-free conditions. The development of the reaction was monitored by applying TLC. At the end of the reaction, hot ethanol (10 mL) was added to the reaction mixture, and the magnetic catalyst was separated by an external magnet. Finally, the pure product was obtained by recrystallization from ethanol.

**2.3.2. Procedure for the recovery of  $\text{Fe}_3\text{O}_4@\text{FSM-16}/\text{IL-Pd}$ .**  $\text{Fe}_3\text{O}_4@\text{FSM-16}/\text{IL-Pd}$  (0.006 g) was added to a mixture of benzaldehyde (1 mmol), malononitrile (1 mmol), and 4-hydroxycoumarin (1 mmol) at 70 °C. After 10 min, hot ethanol (10 mL) was added and the catalyst was separated using an external magnet. The recovered nanocatalyst was then washed with ethanol, dried, and reused in the subsequent runs.

## 3. Results and discussion

### 3.1. Synthesis and characterization of the catalyst

To prepare  $\text{Fe}_3\text{O}_4@\text{FSM-16}/\text{IL-Pd}$  nanocatalyst, firstly,  $\text{Fe}_3\text{O}_4@\text{FSM-16}$  was prepared by the reported method.<sup>53</sup> Next,  $\text{IL}_{\text{DABCO}}$  (bis-PrSi/DABCO/Cl) was synthesized using the reaction of 1,4-diazabicyclo[2.2.2]octane (DABCO) with 3-chloropropyltrimethoxysilane (CPTMS). In the following, the  $\text{IL}_{\text{DABCO}}$  was stabilized on the  $\text{Fe}_3\text{O}_4@\text{FSM-16}$  surface through an organosiloxane bridge with free surface chloride ions. Finally,  $\text{Fe}_3\text{O}_4@\text{FSM-16}/\text{IL}$  was then reacted with  $\text{PdCl}_2$  to prepare  $\text{Fe}_3\text{O}_4@\text{FSM-16}/\text{IL-Pd}$  nanocatalyst (Scheme 1). The synthesized heterogeneous catalyst was characterized by various methods including FT-IR, FE-SEM, XRD, TGA, TEM, BET, EDX, and VSM analyses.

Fig. 1 displays the FT-IR spectra of  $\text{Fe}_3\text{O}_4$ ,  $\text{Fe}_3\text{O}_4@\text{FSM-16}$ ,  $\text{Fe}_3\text{O}_4@\text{FSM-16}/\text{IL}$ ,  $\text{Fe}_3\text{O}_4@\text{FSM-16}/\text{IL-Pd}$ , and reused  $\text{Fe}_3\text{O}_4@\text{FSM-16}/\text{IL-Pd}$ . The peaks observed at 578 and 3400  $\text{cm}^{-1}$  are corresponded to the Fe-O and O-H bonds, respectively (Fig. 1a).<sup>39</sup> This band confirms the presence of iron oxide in all samples (Fig. 1a, b, c, e and f). The bands appeared in Fig. 1b at 806 and 1106  $\text{cm}^{-1}$  have been identified as the asymmetric and symmetric stretching vibrations of Si-O-Si, and the broad band at 3385  $\text{cm}^{-1}$  was attributed to the Si-OH stretching vibration, which confirms the successful coating of FSM-16 onto  $\text{Fe}_3\text{O}_4$ . After the  $\text{Fe}_3\text{O}_4@\text{FSM-16}/\text{IL}$  synthesis, the new absorption band appeared at 2850  $\text{cm}^{-1}$  is related to the  $\text{CH}_2$  groups, and the appearing peak at 1466  $\text{cm}^{-1}$  indicates the presence of quaternary amine.<sup>72</sup> Finally, the FT-IR spectrum of  $\text{Fe}_3\text{O}_4@\text{FSM-16}/\text{IL-Pd}$  (Fig. 1d) confirms the successful immobilization of the mesoporous shell of FSM-16 and IL onto magnetite NPs. Also, the fresh catalyst was compared with the recycled catalyst, and no significant change was observed in their FT-IR spectra,

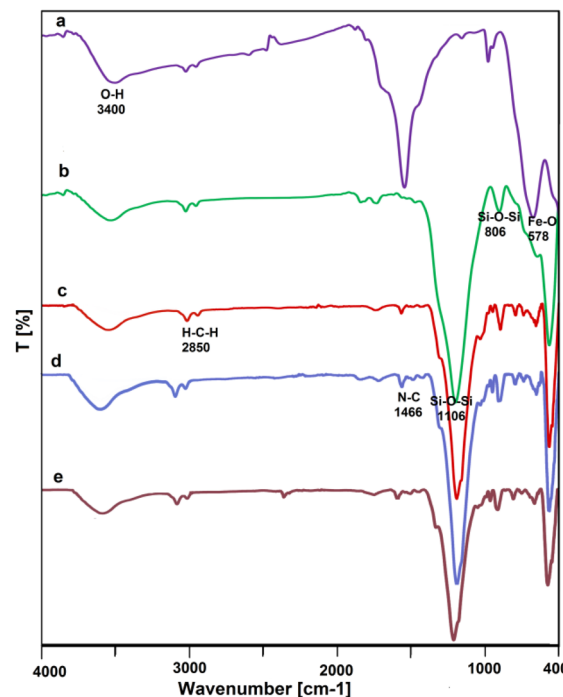


Fig. 1 The FT-IR spectra of (a)  $\text{Fe}_3\text{O}_4$ , (b)  $\text{Fe}_3\text{O}_4@\text{FSM-16}$ , (c)  $\text{Fe}_3\text{O}_4@\text{FSM-16}/\text{IL}$ , (d)  $\text{Fe}_3\text{O}_4@\text{FSM-16}/\text{IL-Pd}$ , and (e) recycled  $\text{Fe}_3\text{O}_4@\text{FSM-16}/\text{IL-Pd}$ .

confirming the structure and stability of the catalyst after recycling (Fig. 1d and e).

The wide-angle powder X-ray diffraction of FSM-16,  $\text{Fe}_3\text{O}_4$ ,  $\text{Fe}_3\text{O}_4@\text{FSM-16}$ ,  $\text{Fe}_3\text{O}_4@\text{FSM-16}/\text{IL-Pd}$ , and (e) reused  $\text{Fe}_3\text{O}_4@\text{FSM-16}/\text{IL-Pd}$  were investigated within the range of  $2\theta = 10\text{--}80^\circ$

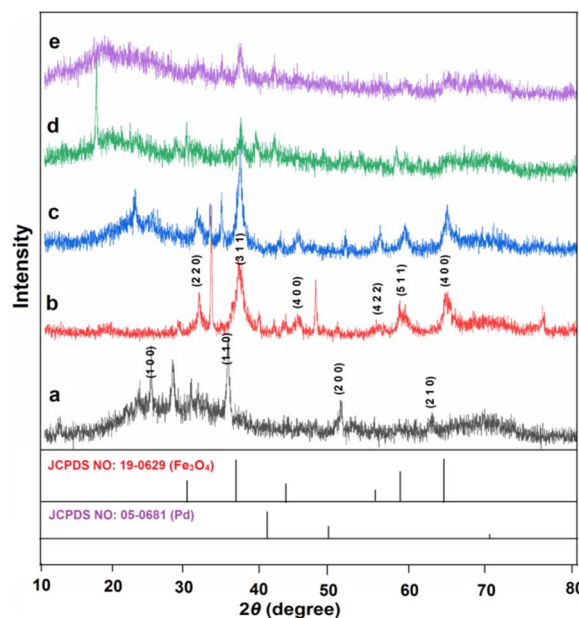


Fig. 2 XRD patterns of (a) FSM-16, (b)  $\text{Fe}_3\text{O}_4$ , (c)  $\text{Fe}_3\text{O}_4@\text{FSM-16}$ , (d)  $\text{Fe}_3\text{O}_4@\text{FSM-16}/\text{IL-Pd}$ , and (e) recycled  $\text{Fe}_3\text{O}_4@\text{FSM-16}/\text{IL-Pd}$ .





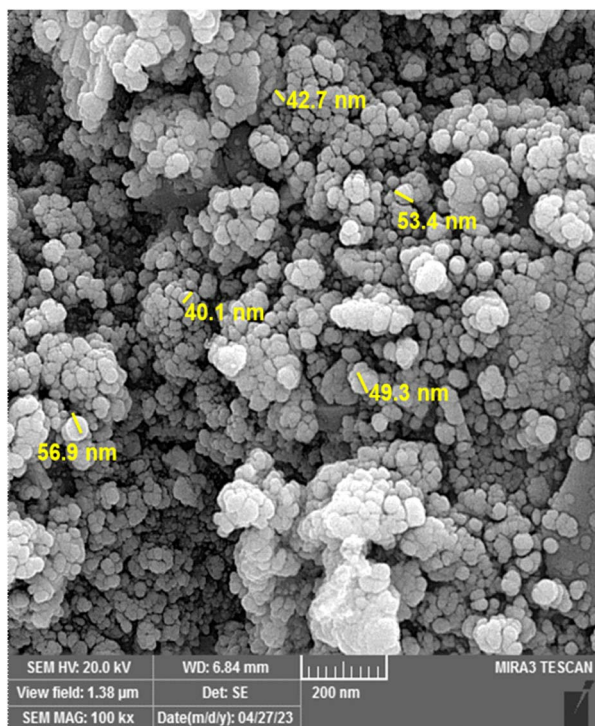


Fig. 3 The FE-SEM image of  $\text{Fe}_3\text{O}_4@\text{FSM-16/IL-Pd}$  nanocatalyst.

(Fig. 2). Based on Fig. 2a, four signals are present at  $2\theta = 23.4^\circ$ ,  $37.1^\circ$ ,  $48.5^\circ$ , and  $61.5^\circ$ , respectively attributed to the 1 0 0, 1 1 0, 2 0 0, and 2 1 0 planes of the regular hexagonal FSM-16.<sup>54</sup> The spinel structure of  $\text{Fe}_3\text{O}_4$  exhibits six signals at  $2\theta$  values of  $30.26^\circ$ ,  $35.7^\circ$ ,  $43.5^\circ$ ,  $53.59^\circ$ ,  $57.5^\circ$  and  $63.26^\circ$ , which assigned to planes of 2 2 0, 3 1 1, 4 0 0, 4 2 2, 5 1 1 and 4 4 0, respectively (Fig. 2b).<sup>39,54</sup> The XRD analysis of  $\text{Fe}_3\text{O}_4@\text{FSM-16}$  depicted in Fig. 2c is in agreement with the typical magnetite pattern of  $\text{Fe}_3\text{O}_4$  coated FSM-16. In addition, the reduction and

modification of the peak intensity of the  $\text{Fe}_3\text{O}_4@\text{FSM-16/IL-Pd}$  nanocatalyst, compared to different synthesis steps, successfully indicate the stabilization of FSM-16, the ionic liquid, and Pd on the  $\text{Fe}_3\text{O}_4$  NPs (Fig. 2d). X-ray diffraction spectrum of the recycled catalyst confirms its maintained structure, efficacy, and thermal stability after recycling (Fig. 2e).

As depicted in Fig. 3, the morphology of the surface, structural characteristics, and particle size details of the  $\text{Fe}_3\text{O}_4@\text{FSM-16/IL-Pd}$  nanocatalyst was evaluated by field effect scanning electron microscopy (FE-SEM). The FE-SEM image shows that the synthesized nanocatalyst has a spherical morphology and regularity. Based on the images, the particle size distribution was about 40–56 nm.

In addition, the chemical purity and distribution of the elements of the  $\text{Fe}_3\text{O}_4@\text{FSM-16/IL-Pd}$  structure were performed by the energy dispersive X-ray (EDX) technique (Fig. S1, ESI†). The results shows the presence of Fe, C, O, N, Si, Cl, and Pd elements in  $\text{Fe}_3\text{O}_4@\text{FSM-16/IL-Pd}$  catalyst, and confirms the successful immobilization of ionic liquid and Pd on FSM-16 magnetite nanoparticles.

The transmission electron microscopy (TEM) image of  $\text{Fe}_3\text{O}_4@\text{FSM-16/IL-Pd}$  magnetic nanocatalyst is shown in Fig. 4. The TEM image confirm the core-shell structure, revealing that the black cores of  $\text{Fe}_3\text{O}_4$  are encompassed by a grey shell of FSM-16/IL-Pd. Additionally, the presence of some small dark spots observed in image could be ascribed to the Pd NPs within the catalyst. The histogram of the palladium particle size distribution revealed a size range of 1.5 to 4.5 nm.

Furthermore, considering the physicochemical and structural parameters of the  $\text{Fe}_3\text{O}_4@\text{FSM-16/IL-Pd}$  nanocatalyst, nitrogen adsorption-desorption isotherms were measured (Fig. S2, ESI†). According to the IUPAC classification, the  $\text{N}_2$  adsorption-desorption isotherm of the acquired catalyst conforms to type IV, confirming the existence of mesoporous silica structures. Following the results analysis, the surface area, total pore volume, and mean pore diameter of the  $\text{Fe}_3\text{O}_4@\text{FSM-16/IL-Pd}$  nanocatalyst were determined.

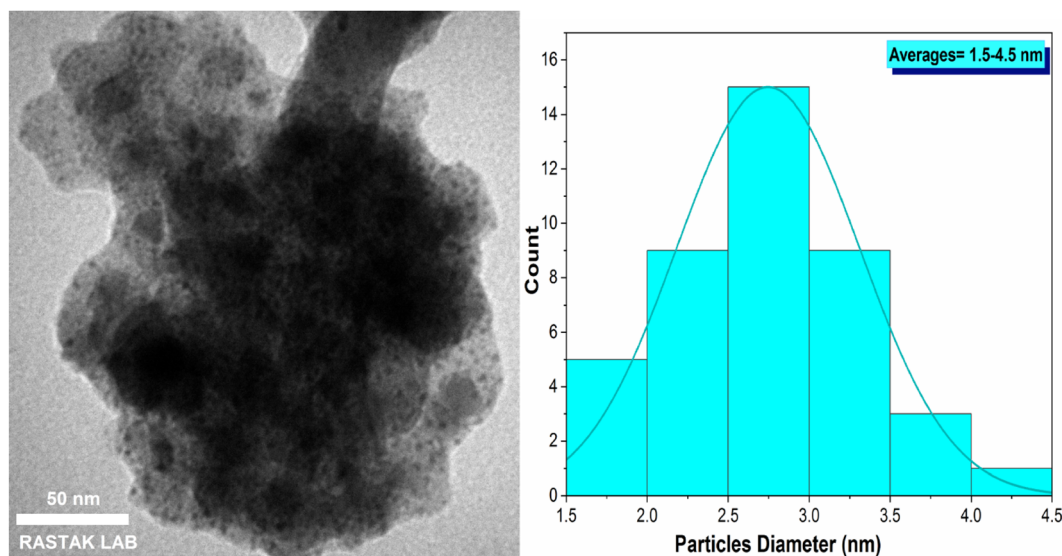


Fig. 4 The TEM images of  $\text{Fe}_3\text{O}_4@\text{FSM-16/IL-Pd}$  nanocatalyst.



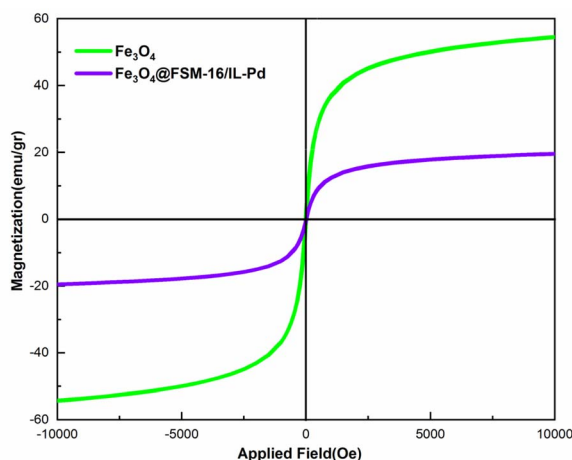


Fig. 5 VSM analysis of the  $\text{Fe}_3\text{O}_4$  and  $\text{Fe}_3\text{O}_4@FSM-16/IL-Pd$ .

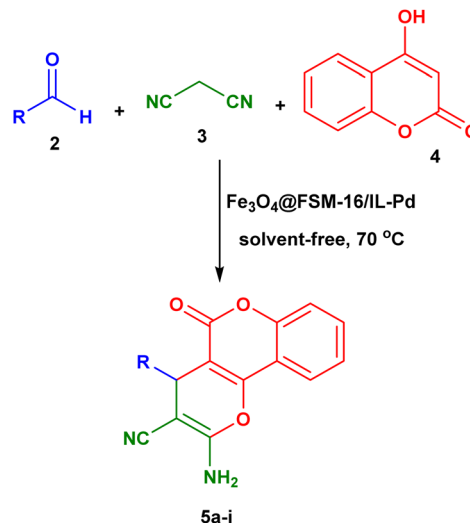
$16/IL-Pd$  nanocatalyst were determined at  $197 \text{ m}^2 \text{ g}^{-1}$ ,  $0.07 \text{ cm}^3 \text{ g}^{-1}$ , and  $8.56 \text{ nm}$ , respectively.

The thermal stability of the  $\text{Fe}_3\text{O}_4@FSM-16/IL-Pd$  nanocatalyst was investigated *via* thermal gravimetric analysis (TGA) within the temperature range of  $25\text{--}900^\circ\text{C}$  (Fig. S3, ESI†). The TGA spectrum indicates an initial weight loss of approximately 4% at a temperature below  $230^\circ\text{C}$ . This weight loss can be attributed to the removal of organic solvents, water, surface hydroxyl groups, and physically and chemically absorbed moisture on the surface of the nanocatalyst. The greatest and second weight loss between  $230\text{--}550^\circ\text{C}$  about 46% is related to the thermal decomposition of the DABCO bridge, organic groups, and complexes, as well as the amine groups present on the surface of the  $\text{Fe}_3\text{O}_4@FSM-16/IL-Pd$  nanocomposite. Finally, the complete thermal decomposition of the nanocatalyst framework is confirmed by a weight loss of about 7% at  $550$  and  $900^\circ\text{C}$ , which validates its stability in catalytic applications.

The magnetic characteristics of  $\text{Fe}_3\text{O}_4$  and  $\text{Fe}_3\text{O}_4@FSM-16/IL-Pd$  were studied using a vibrating sample magnetometer (VSM) at room temperature (Fig. 5). According to the VSM curves, the magnetic saturation values for  $\text{Fe}_3\text{O}_4$  and  $\text{Fe}_3\text{O}_4@FSM-16/IL-Pd$  are  $53$  and  $19.5 \text{ emu g}^{-1}$ , respectively. The results show that the synthesized samples have superparamagnetic properties and the decrease in magnetization of  $\text{Fe}_3\text{O}_4@FSM-16/IL-Pd$ , as compared to  $\text{Fe}_3\text{O}_4$ , can be attributed to the immobilization of the coated FSM-16, ionic liquid, and Pd around the  $\text{Fe}_3\text{O}_4$  NPs. However, the magnetic sensitivity of nanocatalyst is sufficient for its easy magnetic recovery from various reaction mixtures. Therefore, the prepared catalyst can be readily recovered using magnets.

### 3.2. Synthesis of pyrano[3,2-*c*]chromene-3-carbonitrile derivatives

The catalytic performance of  $\text{Fe}_3\text{O}_4@FSM-16/IL-Pd$  nanocatalyst was investigated by selecting the three-component reaction of aldehydes, malononitrile, 4-hydroxycoumarin in the synthesis of pyrano[3,2-*c*]chromene-3-carbonitrile derivatives (Scheme 2).



Scheme 2 Synthesis of pyrano[3,2-*c*]chromene-3-carbonitriles using  $\text{Fe}_3\text{O}_4@FSM-16/IL-Pd$  nanocatalyst.

To determine the optimum conditions, the reaction between benzaldehyde ( $1 \text{ mmol}$ ), malononitrile ( $1 \text{ mmol}$ ) and 4-hydroxycoumarin ( $1 \text{ mmol}$ ) was chosen as a model reaction, and various parameters such as the amount of the catalyst, the influence of temperature, and the use of solvents or solvent-free conditions were studied (Table 1). Firstly, the effect of catalyst amount on the reaction model was investigated. The achieved results showed that the effect of catalyst loading has an important role in the progress of the reaction and the best result was obtained in the presence of  $0.006 \text{ g}$  of the  $\text{Fe}_3\text{O}_4@FSM-16/IL-Pd$ . Then, the effect of various solvents was investigated to test the model reaction, and the highest yield was observed under solvent-free conditions. Furthermore, the assessment of other polar and non-polar solvents such as EtOH,  $\text{H}_2\text{O}$ , DMSO,  $\text{CH}_3\text{CN}$ , EtOH/ $\text{H}_2\text{O}$ , and toluene has demonstrated that the

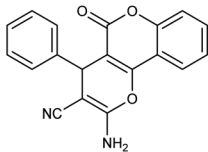
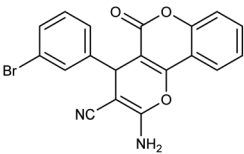
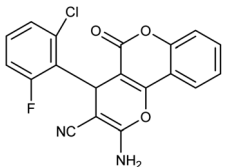
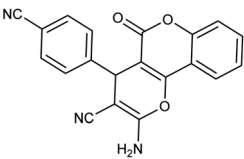
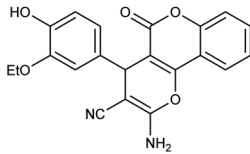
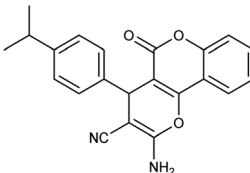
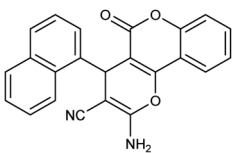
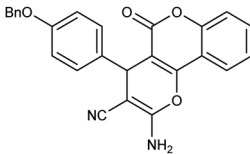
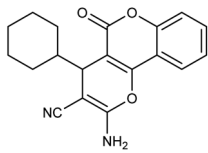
Table 1 Optimization of the reaction conditions for the synthesis of **5a**<sup>a</sup>

Entry	Catalyst loading (g)	Solvent	Temp. ( $^\circ\text{C}$ )	Yield <sup>b</sup> (%)
1	Cat. 1 (0.002)	—	70	45
2	Cat. 1 (0.004)	—	70	55
3	Cat. 1 (0.006)	—	70	96
4	Cat. 1 (0.008)	—	70	96
5	Cat. 1 (0.006)	EtOH	70	55
6	Cat. 1 (0.006)	$\text{H}_2\text{O}$	70	60
7	Cat. 1 (0.006)	EtOH/ $\text{H}_2\text{O}$	70	55
8	Cat. 1 (0.006)	$\text{CH}_3\text{CN}$	70	50
9	Cat. 1 (0.006)	DMSO	70	45
10	Cat. 1 (0.006)	Toluene	70	35
11	Cat. 1 (0.006)	Solvent-free	25	50
12	Cat. 1 (0.006)	Solvent-free	40	60
13	Cat. 1 (0.006)	Solvent-free	80	65
14	$\text{Fe}_3\text{O}_4@FSM-16$ (0.006)	Solvent-free	70	40
15	$\text{Fe}_3\text{O}_4@FSM-16/IL$ (0.006)	Solvent-free	70	50

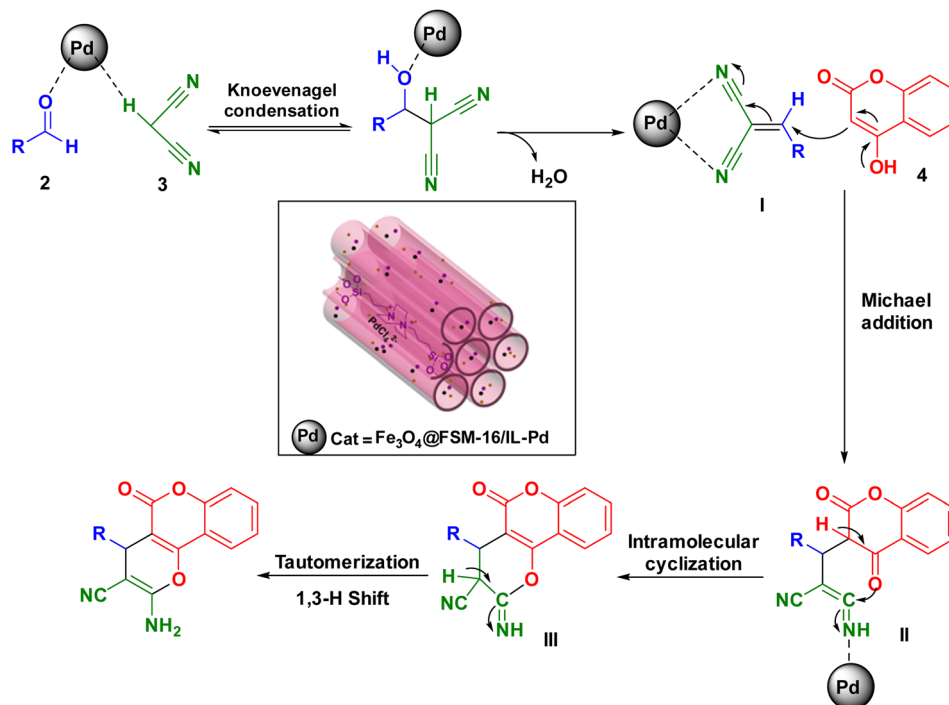
<sup>a</sup> Reaction conditions: benzaldehyde ( $1 \text{ mmol}$ ), malononitrile ( $1 \text{ mmol}$ ), 4-hydroxycoumarin ( $1 \text{ mmol}$ ), time:  $20 \text{ min}$ . <sup>b</sup> Isolated yields.



Table 2 Synthesis of 5a–i using Fe<sub>3</sub>O<sub>4</sub>@FSM-16/IL-Pd nanocatalyst<sup>a</sup>

Entry	Aldehyde	Product 5	Yield <sup>b</sup> (%)
5a	C <sub>6</sub> H <sub>5</sub> CHO		97 (ref. 76)
5b	3-Br-C <sub>6</sub> H <sub>4</sub> CHO		92 (ref. 76)
5c	2-Cl-6-F-C <sub>6</sub> H <sub>3</sub> CHO		93 (ref. 76)
5d	4-CN-C <sub>6</sub> H <sub>4</sub> CHO		92 (ref. 5)
5e	3-OEt-4-OH-C <sub>6</sub> H <sub>3</sub> CHO		95 (ref. 76)
5f	4-Isopropyl-C <sub>6</sub> H <sub>4</sub> CHO		96 (ref. 76)
5g	1-Naphthaldehyde		92 (ref. 76)
5h	4-BnO-C <sub>6</sub> H <sub>4</sub> CHO		93 (ref. 76)
5i	Cyclohexanecarbaldehyde		92 (ref. 76)

<sup>a</sup> Reaction conditions: aldehyde (1 mmol), malononitrile (1 mmol), 4-hydroxycoumarin (1 mmol), Fe<sub>3</sub>O<sub>4</sub>@FSM-16/IL-Pd (0.006 g), solvent-free, 70 °C. Time: 10–15 min. <sup>b</sup> Isolated yields.



Scheme 3 Proposed mechanism for the synthesis of 5 in the presence of nanocatalyst 1.

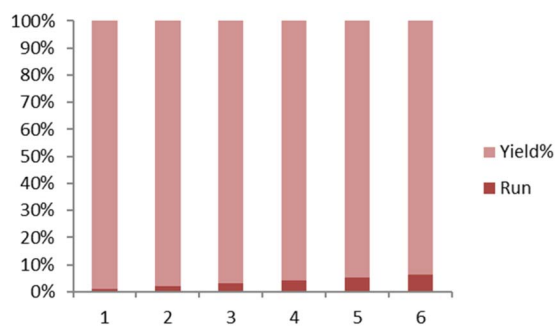


Fig. 6 Reusability of the  $\text{Fe}_3\text{O}_4\text{@FSM-16/IL-Pd}$  nanocatalyst.

reaction time is lengthier, and the yield of the final product is reduced. In the next study, the effect of the temperature was investigated and the best result was obtained at 70 °C. Also, to indicate the effect of the catalytic activity  $\text{Fe}_3\text{O}_4\text{@FSM-16/IL-Pd}$ ,

the catalytic performance of  $\text{Fe}_3\text{O}_4\text{@FSM-16}$  and  $\text{Fe}_3\text{O}_4\text{@FSM-16/IL}$  were studied as shown in Table 1. Table 1 demonstrates that  $\text{Fe}_3\text{O}_4\text{@FSM-16/IL-Pd}$  exhibits greater activity than its precursor catalysts in the model reaction and when the  $\text{Fe}_3\text{O}_4\text{@FSM-16}$  and  $\text{Fe}_3\text{O}_4\text{@FSM-16/IL}$  were employed as catalysts, moderate yields were obtained. Finally, the use of 0.006 g of  $\text{Fe}_3\text{O}_4\text{@FSM-16/IL-Pd}$  and solvent-free conditions at 70 °C was determined as the optimum conditions.

Following optimization, various aldehydes including electron-donating, and electron-accepting groups were examined to synthesize the pyrano[3,2-*c*]chromene-3-carbonitriles. As shown in Table 2, the variety of pyrano[3,2-*c*]chromene-3-carbonitrile derivatives were successfully synthesized with good to excellent yields at short reaction times.

The suggested mechanism for the synthesis of pyrano[3,2-*c*]chromenes using  $\text{Fe}_3\text{O}_4\text{@FSM-16/IL-Pd}$  is shown in Scheme 3. Initially, the carbonyl group of the aldehyde is activated by the Lewis acid site of the catalyst through coordination, which

Table 3 Comparison of the efficiency of the  $\text{Fe}_3\text{O}_4\text{@FSM-16/IL-Pd}$  with other catalysts in the synthesis of pyrano[3,2-*c*]chromene-3-carbonitrile

Catalyst	Experimental conditions	Yield <sup>a</sup> (%)
[Bmim]BF <sub>4</sub> (4 mmol)	Solvent-free, 70 °C, 240 min	88 (ref. 75)
SSMA (5 mol%)	EtOH:H <sub>2</sub> O, 90 °C, 40 min	94 (ref. 76)
Sodiumdodecyl sulfate (20 mol%)	H <sub>2</sub> O, 60 °C, 150 min	81 (ref. 77)
[DMAP-PEG1000-DIL][BF <sub>4</sub> ] (0.01 mmol)	H <sub>2</sub> O, 100 °C, 30 min	92 (ref. 78)
<i>o</i> -Benzenedisulfonimide (50 mol%)	Solvent-free, 120 °C, 50 min	85 (ref. 79)
$\text{Fe}_3\text{O}_4\text{@FSM-16/IL-Pd}$ (0.57 mol%)	Solvent-free, 70 °C, 10 min	97 <sup>b</sup>

<sup>a</sup> Isolated yields. <sup>b</sup> This work.



accelerates the condensation step. Afterward, the activated aldehyde is attacked by the active methylene of malononitrile to give  $\alpha,\beta$ -unsaturated intermediate **I** via the Knoevenagel condensation, and elimination of a water molecule. Next, a Michael 1,4-addition reaction between 4-hydroxycoumarin and the activated intermediate **I** leads to the formation of intermediate **II**. Finally, the intramolecular cyclization of intermediate **II** to intermediate **III** and its tautomerization (1,3-H shift) gives the corresponding products.<sup>73,74</sup>

### 3.3. Efficiency of the catalyst

The leaching test was conducted to confirm the heterogeneous nature of the  $\text{Fe}_3\text{O}_4\text{@FSM-16/IL-Pd}$  catalyst during the synthesis of pyrano[3,2-*c*]chromene-3-carbonitrile. Based on this, the model reaction was investigated using the optimized reaction conditions. After the progress of approximately 50%, the catalyst was removed from the reaction. Afterward, the residue of the reaction was stirred under optimal conditions without the presence of the catalyst. However, no significant increase in product conversion was observed. The results of this experiment were checked using the ICP-MS technique and it confirms that the catalyst is heterogeneous and minimal washing of Pd catalytic centers occurs during the reaction (less than 1.3%). The reusability of the catalyst was investigated in the model reaction under optimal reaction conditions. After completion of the reaction, the heterogeneous catalyst was magnetically separated, washed with EtOH and  $\text{H}_2\text{O}$ , and dried for use in the next run. As shown in Fig. 6, the recycled catalyst was used for five runs with no significant loss in performance.

Finally, to evaluate the performance of the  $\text{Fe}_3\text{O}_4\text{@FSM-16/IL-Pd}$  catalyst, it was compared with other previously reported catalysts for the synthesis of pyrano[3,2-*c*]chromene-3-carbonitrile derivatives. According to the results in Table 3, the  $\text{Fe}_3\text{O}_4\text{@FSM-16/IL-Pd}$  heterogeneous catalyst is more effective than the other catalysts studied in terms of the amount of catalyst, reaction temperature, reaction time, product yield, and type of solvent.

## 4. Conclusions

In this research,  $\text{Fe}_3\text{O}_4\text{@FSM-16/IL-Pd}$  as a new catalyst was synthesized and characterized. This nanocomposite was prepared via the immobilization of ionic liquid on the surface of magnetite nanoparticles coated by FSM-16, which possess a high capacity for stabilizing Pd ions. The physical characteristics of this nanocatalyst were examined via various techniques including FT-IR, TGA, TEM, EDX, FE-SEM, BET, VSM, and XRD analysis.  $\text{Fe}_3\text{O}_4\text{@FSM-16/IL-Pd}$  nanocatalyst was effectively used to synthesize diverse pyrano[3,2-*c*]chromene-3-carbonitrile derivatives via the condensation of aldehydes, malononitrile, and 4-hydroxycoumarin under solvent-free condition. Moreover, the magnetically nanocatalyst can be easily separated from the reaction mixture using an external magnet and can be reused five times without a significant loss in its catalytic activity. Also, the recycled catalyst was characterized using SEM,

TGA, TEM, XRD, FT-IR, and VSM analyses, which revealed the high stability of the catalyst under optimal reaction conditions.

## Conflicts of interest

There are no conflicts to declare.

## Acknowledgements

The authors gratefully acknowledge the partial support of this work by Yasouj University, Iran.

## Notes and references

- 1 T. M. Dhameliya, H. A. Donga, P. V. Vaghela, B. G. Panchal, D. K. Sureja, K. B. Bodiwala and M. T. A. Chhabria, *RSC Adv.*, 2020, **10**, 32740.
- 2 A. M. El-Agrody, A. M. Fouda, M. A. Assiri, A. Mora, T. E. Ali, M. M. Alam and M. Y. Alfaifi, *Med. Chem. Res.*, 2020, **29**, 617.
- 3 N. A. Al-Masoudi, H. H. Mohammed, A. M. Hamdy, O. A. Akrawi, N. Eleya, A. Spannenberg, C. Pannecouque and P. Langer, *Z. Naturforsch. B*, 2013, **68**, 229.
- 4 N. Arif, Z. Shafiq, K. Mahmood, M. Rafiq, S. Naz, S. A. Shahzad, U. Farooq, A. H. Bahkali, A. M. Elgorban, M. Yaqub and A. El-Gokha, *ACS Omega*, 2022, **7**, 28605.
- 5 A. Kakanejadifard, F. Azarban, N. Khosravani and B. Notash, *J. Mol. Liq.*, 2016, **221**, 211.
- 6 M. Rueping, E. Sugiono and E. Merino, *Chem. - Eur. J.*, 2008, **14**, 6329.
- 7 H. Ostadzadeh and H. Kiyani, *Polycyclic Aromat. Compd.*, 2023, **43**, 9318.
- 8 S. Banerjee and A. Saha, *New J. Chem.*, 2013, **37**, 4170.
- 9 M. Jarrahi, B. Maleki and R. Tayeb, *RSC Adv.*, 2022, **12**, 28886.
- 10 H. Boroumand, H. Alinezhad, B. Maleki and S. Peiman, *Polycyclic Aromat. Compd.*, 2022, **43**, 7853.
- 11 A. R. Nesaragi, T. V. Gasti, T. A. Metre, A. Anand, R. R. Kamble, R. B. Chougale and R. S. Keri, *ChemistrySelect*, 2022, **7**, e202200604.
- 12 P. Kate, V. Pandit, V. Jawale and M. Bachute, *J. Chem. Sci.*, 2022, **134**, 1.
- 13 M. Bayzidi and B. Zeynizadeh, *ChemistrySelect*, 2022, **7**, e202202708.
- 14 A. Chelihi, R. Hassaine, S. Nachat, M. Benabdallah, K. Bendahou, M. Aissaoui and M. Saidj, *J. Heterocycl. Chem.*, 2024, **61**, 439.
- 15 A. Benrashid, D. Habibi, M. Beiranvand and M. Mahmoudiani Gilan, *Sci. Rep.*, 2023, **13**, 17608.
- 16 P. Gómez-López, A. Puente-Santiago, A. Castro-Beltrán, L. A. S. do Nascimento, A. M. Balu, R. Luque and C. G. Alvarado-Beltrán, *Curr. Opin. Green Sustainable Chem.*, 2020, **24**, 48.
- 17 P. Gupta and S. Paul, *Catal. Today*, 2014, **236**, 153.
- 18 M. J. Climent, A. Corma and S. Iborra, *RSC Adv.*, 2012, **2**, 16.
- 19 L. V. Chopda and P. N. Dave, *ChemistrySelect*, 2020, **5**, 5552.
- 20 C. M. Hendrich, K. Sekine, T. Koshikawa, K. Tanaka and A. S. K. Hashmi, *Chem. Rev.*, 2020, **121**, 9113.



- 21 H. Lee, X. Wu and L. Sun, *Nanoscale*, 2020, **12**, 4187.
- 22 A. Bavykina, N. Kolobov, I. S. Khan, J. A. Bau, A. Ramirez and J. Gascon, *Chem. Rev.*, 2020, **120**, 8468.
- 23 C. Dong, Y. Li, D. Cheng, M. Zhang, J. Liu, Y. G. Wang, D. Xiao and D. Ma, *ACS Catal.*, 2020, **10**, 11011.
- 24 H. Veisi, A. Sedrpoushan and S. Hemmati, *Appl. Organomet. Chem.*, 2015, **29**, 825.
- 25 A. Barzkar, A. Salimi Beni, S. Parang and F. Salahshour, *Sci. Rep.*, 2023, **13**, 19940.
- 26 M. Mohammadi and A. Ghorbani-Choghamarani, *New J. Chem.*, 2020, **44**, 2919.
- 27 H. Al-shaikh, J. Lasri, J. G. Knight and S. T. Al-Goul, *Fuel*, 2022, **325**, 124962.
- 28 L. Bi, Y. Teng, M. Baghayeri and J. Bao, *Environ. Res.*, 2023, **237**, 117030.
- 29 L. M. Rossi, N. J. Costa, F. P. Silva and R. Wojcieszak, *Green Chem.*, 2014, **16**, 2906.
- 30 Y. Zhu, L. P. Stubbs, F. Ho, R. Liu, C. P. Ship, J. A. Maguire and N. S. Hosmane, *ChemCatChem*, 2010, **2**, 365.
- 31 M. Kazemi and M. Mohammadi, *Appl. Organomet. Chem.*, 2020, **34**, 5400.
- 32 S. Shylesh, V. Schünemann and W. R. Thiel, *Angew. Chem., Int. Ed.*, 2010, **49**, 3428.
- 33 V. Polshettiwar, R. Luque, A. Fihri, H. Zhu, M. Bouhrara and J. M. Basset, *Chem. Rev.*, 2011, **111**, 3036.
- 34 M. Hajjami, L. Shiri and A. Jahanbakhshi, *Appl. Organomet. Chem.*, 2015, **29**, 668.
- 35 D. Wang, S. Li, C. Wu and T. Li, *J. Am. Chem. Soc.*, 2020, **144**, 685.
- 36 M. Chellappa and U. Vijayalakshmi, *Mater. Today: Proc.*, 2019, **9**, 371.
- 37 S. Keshipour and A. Al-Azmi, *Appl. Organomet. Chem.*, 2020, **34**, 5311.
- 38 R. Saberi and M. Nasr-Esfahani, *J. Cluster Sci.*, 2023, **34**, 2609.
- 39 A. Jahanbakhshi and M. Farahi, *Arabian J. Chem.*, 2022, **15**, 104311.
- 40 A. Jahanbakhshi and M. Farahi, *Monatsh. Chem.*, 2023, **154**, 249.
- 41 A. Jahanbakhshi, M. Farahi and Y. Aghajani, *Acta Chim. Slov.*, 2022, **69**, 837.
- 42 P. Moradi and M. Hajjami, *RSC Adv.*, 2022, **12**, 13523.
- 43 N. Y. Baran, T. Baran, M. Nasrollahzadeh and R. S. Varma, *J. Organomet. Chem.*, 2019, **900**, 120916.
- 44 S. Vaidya, P. Thaplyal, K. Ramanujachary, S. Lofland and A. K. Ganguli, *J. Nanosci. Nanotechnol.*, 2011, **11**, 3405.
- 45 X. Shi, S. Quan, L. Yang, G. Shi and F. Shi, *Chemosphere*, 2019, **219**, 914.
- 46 J. Dai, H. Zou, R. Wang, Y. Wang, Z. Shi and S. Qiu, *Green Chem.*, 2017, **19**, 1336.
- 47 J. A. S. Costa, R. V. M. Oliveira, L. P. C. Romão and C. M. Paranhos, *ACS Appl. Energy Mater.*, 2023, **1**, 2417.
- 48 R. Vinayagam, C. Zhou, S. Pai, T. Varadavenkatesan and M. K. Narasimhan, *Mater. Chem. Phys.*, 2021, **262**, 124323.
- 49 S. Ehsanimehr, P. N. Moghadam, W. Dehaen and V. Shafiei-Irannejad, *Colloids Surf., A*, 2021, **615**, 126302.
- 50 R. Rafieenezhad, A. Izadbakhsh and A. M. Sanati, *J. Porous Mater.*, 2021, **28**, 1749.
- 51 A. Hosseini and H. Faghihian, *Ind. Eng. Chem. Res.*, 2019, **76**, 122.
- 52 T. Selvam, M. Köstner, G. T. P. Mabande, W. Schwieger, N. Pfänder and R. Schlögl, *J. Porous Mater.*, 2007, **14**, 263.
- 53 A. Jahanbakhshi and M. Farahi, *RSC Adv.*, 2023, **13**, 31252.
- 54 A. Jahanbakhshi, M. Farahi, B. Karami and I. Sedighimehr, *RSC Adv.*, 2022, **12**, 34325.
- 55 A. Jahanbakhshi, S. Eskandari and M. Farahi, *New J. Chem.*, 2024, **48**, 1381.
- 56 F. Gholamian, M. Hajjami and A. M. Sanati, *Silicon*, 2020, **12**, 2121.
- 57 S. Hashemi-Uderji, M. Abdollahi-Alibeik and R. Ranjbar-Karimi, *J. Porous Mater.*, 2019, **26**, 467.
- 58 M. Samari, S. Zinadini, A. A. Zinatizadeh, M. Jafarzadeh and F. A. Gholami, *J. Environ. Chem. Eng.*, 2021, **9**, 105386.
- 59 S. Hashemi-Uderji and M. Abdollahi-Alibeik, *J. Iran. Chem. Soc.*, 2018, **15**, 1709.
- 60 W. Cao, L. Tan, H. Wang and J. Yuan, *ACS Macro Lett.*, 2021, **10**, 161.
- 61 K. Jie, N. Onishi, J. A. Schott, I. Popovs, D. E. Jiang, S. Mahurin and S. Dai, *Angew. Chem.*, 2020, **132**, 2288.
- 62 M. Nasrollahzadeh, N. Motahharifar, Z. Nezafat and M. Shokouhimehr, *J. Mol. Liq.*, 2021, **341**, 117398.
- 63 L. A. Bischoff, M. Drisch, C. Kerpen, P. T. Hennig, J. Landmann, J. A. Sprenger, R. Bertermann, M. Grüne, Q. Yuan, J. Warneke, X. B. Wang and M. Finze, *Chem. - Eur. J.*, 2019, **25**, 3560.
- 64 S. Rostamnia, E. Doustkhah and B. Zeynizadeh, *Microporous Mesoporous Mater.*, 2016, **222**, 87.
- 65 M. M. Abdullah, A. A. AlQuraishi, H. A. Allohedan, A. O. AlMansou and A. M. Atta, *J. Mol. Liq.*, 2017, **233**, 508.
- 66 S. Sadjadi, P. Mohammadi and M. Heravi, *Sci. Rep.*, 2020, **10**, 6535.
- 67 B. Karimi, F. Mansouri and H. A. Vali, *Green Chem.*, 2014, **16**, 2587.
- 68 H. Wan, W. Zuowang, C. Wen, G. Guofeng, C. Yuan, C. Chong, L. Zhong and L. Xiaoqin, *J. Mol. Catal. A: Chem.*, 2015, **398**, 127.
- 69 M. Jin, Q. Niu, G. Liu, Z. Lv, C. Si and H. Guo, *J. Mater. Sci.*, 2020, **55**, 8199.
- 70 S. Ikurumi, S. Okada, K. Nakatsuka, T. Kamegawa, K. Mori and H. Yamashita, *J. Phys. Chem. C*, 2014, **118**, 575.
- 71 Y. L. Hu, J. R. Li, C. Chen, X. B. Liu and Q. Rong, *Sustainable Chem. Pharm.*, 2022, **29**, 100779.
- 72 J. Davarpanah and A. R. Kiasat, *Catal. Commun.*, 2013, **42**, 98.
- 73 F. Ghobakhloo, D. Azarifar, M. Mohammadi, H. Keypour and H. Zeynali, *Inorg. Chem.*, 2022, **61**, 4825.
- 74 S. Papi, S. Jamehbozorgi, A. Yazdanipour and M. Ramezani, *Inorg. Chem. Commun.*, 2023, **158**, 111538.
- 75 J. M. Khurana and S. Kumar, *Monatsh. Chem.*, 2010, **141**, 561.
- 76 B. Karami and M. Kiani, *Monatsh. Chem.*, 2016, **147**, 1117.
- 77 H. Mehrabi and H. Abusaidi, *J. Iran. Chem. Soc.*, 2010, **7**, 890.
- 78 Y. Wang, H. Ye, G. Zuo and J. Luo, *J. Mol. Liq.*, 2015, **212**, 418.
- 79 B. Maleki, *Org. Prep. Proced. Int.*, 2016, **48**, 30.

